J|A|C|S COMMUNICATIONS

Published on Web 07/15/2010

# Detection of the Photosystem I:Ferredoxin Complex by Backscattering Interferometry

Pierre Sétif,*,† Nathan Harris,‡ Bernard Lagoutte,† Stephen Dotson,‡ and Scot. R Weinberger*,‡

*iBiTec-S, URA CNRS 2096, CEA Saclay, 91191 Gif sur Yvette, France and Molecular Sensing Inc. (MSI), Montara, California 94037*

Received March 16, 2010; E-mail: pierre.setif@cea.fr; sweinberger@molsense.com

***Abstract:*** The dissociation constant $K_d$ of the photosystem I (PSI): ferredoxin complex has been measured by backscattering interferometry (BSI) with cyanobacterial PSI (350 kDa) and ferredoxin (10.5 kDa). The BSI signal, consisting of shifts for interference fringes resulting from a change in refractive index due to complex formation, was monitored as ferredoxin concentration was titrated. $K_d$ values of 0.14−0.38 $\mu$M were obtained with wild-type PSI whereas no complex was detectable with a PSI mutant containing a single mutation (R39Q) in the PsaE extrinsic subunit. These results are in quantitative agreement with previous functional determinations consisting in the detection of fast electron transfer within the complex. They provide evidence that the main contribution for the high affinity binding of ferredoxin to PSI is due to a single region of PsaE comprising arginine 39. They do not support the existence of a secondary binding site that could have escaped functional detection.

During oxygenic photosynthesis, light energy is converted into chemical energy by photosystem I (PSI) and photosystem II. PSI provides a strong reductant, reduced ferredoxin (Fd), which is involved in many metabolic processes such as reduction of $NADP^+$ into NADPH, nitrogen assimilation, and hydrogen production.[1,2] Three-dimensional X-ray structures of cyanobacterial and plant PSIs have been resolved at 2.5 and 3.4 Å, respectively.[3,4] In the context of photobiological energy production, PSI has been recently incorporated in several types of nanoscale devices[5−9] and has been engineered for direct coupling to electrodes[9] or hydrogenase.[10−12] It is essential to identify the Fd docking site(s) in PSI as it is central to the functioning of the photosynthetic machinery as well as to future PSI engineering. The Fd docking site of cyanobacterial PSI has been initially identified at low resolution by modeling,[13] electron microscopy of a covalent Fd:PSI complex,[14] and mutational effects on the kinetics of Fd reduction.[15] These different approaches gave a similar result, with Fd being docked at one side of the stromal ridge made by the three extrinsic PSI stromal subunits PsaC, PsaD, and PsaE. However, this docking model has been recently challenged and different proposals for another site were put forward.[16,17] Independent ways of assessing the Fd docking site(s) and measuring its (their) affinity(ies) are therefore highly desirable, especially as secondary sites could escape functional detection. Backscattering interferometry (BSI), which detects molecular interactions via changes in the mean polarizability of the probed volume (see Supporting Information for a more thorough explanation), has recently been described as a powerful technique for measuring label-free molecular interactions in free solution.[18] We measured by BSI the dissociation constant $K_d$ of the PSI:Fd complex for both wild-type (WT) PSI and a PsaE site-directed mutant with a prototype BSI instrument developed at Molecular Sensing Inc.[19] (Figure S1). These measurements are in complete agreement with the previous $K_d$ determinations based on electron transfer kinetics. The initial proposal for Fd docking on cyanobacterial PSI is also fully supported by the BSI results with no observable secondary Fd site.

The binding of Fd to PSI has been determined by BSI with WT PSI and Fd both purified from the cyanobacterium *Synechocystis* sp. strain PCC6803 (hereafter named *Synechocystis*) (Figure 1, upper part). Fitting these data with a single binding site gives a dissociation constant $K_d$ of 0.38 $\mu$M with no significant fit improvement when considering two sites with different $K_d$'s. A series of BSI titrations with the same proteins and also with a closely related Fd (from the cyanobacterium *Thermosynechococcus elongatus*) gave $K_d$ values comprised between 0.14 and 0.32 $\mu$M (Figure S2, Table in the Supporting Information). Much of our present knowledge about the functional properties of PSI:Fd complexes has been obtained, up to now, from the kinetics of electron transfer (ET) from PSI to Fd. These kinetics, which were studied by laser flash-absorption spectroscopy, corresponds to ET from the terminal

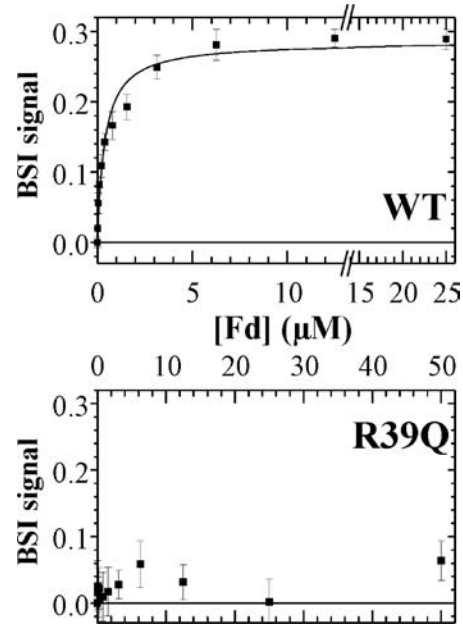


***Figure 1.*** BSI titration curves of complex formation between PSI (10 nM) and Fd. Upper part: WT PSI, Fd from *Synechocystis*. Lower part: PSI mutant (R39Q from PsaE), Fd from *Th. elongatus*. Triplicate measurements were made in 20 mM Tricine pH 8.0, 30 mM NaCl, 5 mM $MgCl_2$, 0.015% (w/v) $\beta$-dodecyl maltoside. The BSI signal is in units of pixels and is representative of the change in refractive index for the binding pairs when compared to the refractive index signal for Fd alone (see Supporting Information for further details).

† iBiTec-S.
‡ MSI.



**10.1021/ja102208u** 

PSI acceptors (two [4Fe-4S] clusters, named $F_A$ and $F_B$, bound to PsaC and undergoing submicrosecond redox equilibrium[20]) to the [2Fe-2S] cluster of ferredoxin. Within the complex, ET is first-order and the amplitude of the corresponding signal can be titrated vs the Fd concentration.[21,22] Dissociation constant $K_d$'s were thus determined, and values of 0.2−0.6 $\mu$M were found for WT *Synechocystis* PSI and Fd from either *Synechocystis*[20] or *Th. elongatus* (see Supporting Information). The $K_d$'s determined here by BSI are therefore fully consistent with these previous measurements.

It is important to note that the ET and BSI measurements were done in quite similar, although not completely identical, redox states of the binding partners (see Supporting Information): In both cases, ($F_A$, $F_B$) and Fd are oxidized, which is crucial for a reliable comparison of the affinities as $K_d$ is probably redox-state dependent.[20,23] The only difference lies in the primary donor P700 of PSI, which is oxidized and reduced in BSI and ET measurements, respectively. However the P700 redox state is not expected to have a significant influence on Fd affinity, as P700 is located at the opposite side of PSI. With P700 being oxidized, the BSI experiments were therefore performed with photochemically inactive PSI.

Functional ET studies were previously performed with a large series of PSI mutants. This revealed that all three extrinsic subunits are essential in the PSI:Fd complex formation and allowed the approximate binding site of Fd to be identified[15] (Figure 2). Among the different mutants, the site-specific mutant R39Q of PsaE was studied in great detail. It was found to exhibit a 250-fold decrease in its binding affinity for Fd. It was also demonstrated that the mutation does not induce any conformational change in the isolated subunit[24] and that the positive charge of the highly exposed Arg is critical for binding Fd.[25] Complex formation between the R39Q mutant and Fd was studied by BSI, with no apparent formation of a complex (Figure 1, lower part and Figure S3). Therefore, the BSI experiments confirm the essential role of R39 of PsaE in Fd binding.

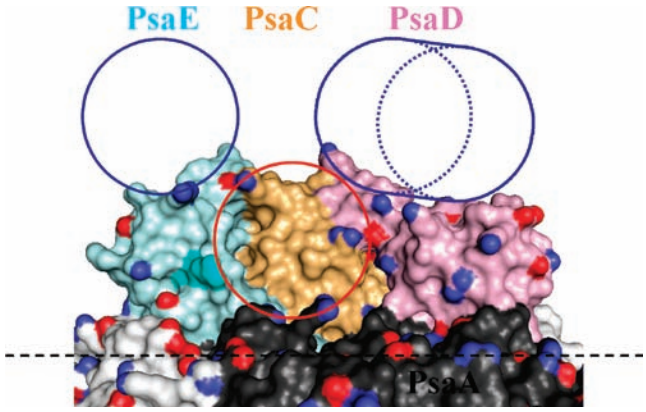


***Figure 2.*** Side view of the stromal ridge of PSI in surface representation (Pymol, V. 0.99[26]). The approximate positions of Fd when docked to PSI (PDB accession code 1JB0.pdb[3]) at the different sites are shown in circles: In red, middle position consistent with the mutational and BSI data; in blue, alternative proposals for Fd positions.[16,17] The membrane level is indicated by a dotted line. Color coding: PsaA, PsaC, PsaD, and PsaE in dark gray, orange, pink, and cyan, respectively; oxygen atoms of acidic side chains in red; nitrogen atoms of basic side chains in blue; residue R39 of PsaE in dark cyan.

The approximate positions of Fd corresponding to the different proposals of PSI binding sites are shown in Figure 2 as circles. The middle position (in red) is the one that was initially proposed and which is in accordance with the present experiments as it is the only one where Fd contacts the essential conserved R39 residue (in cyan). The left top position was found by image analysis of Fd-containing plant-PSI two-dimensional crystals.[16] From modeling of both plant and cyanobacterial PSI,[17] the right top position was recently hypothesized as a second Fd docking site involving essentially subunit PsaD. Our present data give no support to Fd docking with $K_d$ < 30 $\mu$M in these top positions. First-order ET from PSI to Fd within the PSI:Fd cyanobacterial complex was found to be fast and multiphasic with the presence of three exponential components in the submicrosecond and microsecond range.[21] This multiphasic behavior is consistent with the existence of several mutually exclusive complexes[21] which all involve residue R39 of PsaE.[25] The slowest component corresponds to a rate $k_{Fd}$ of Fd reduction of 7000 $s^{-1}$.[20] The solvent-exposed surface of PSI which is consistent with $k_{Fd} \geq 7000$ $s^{-1}$ has been approximately determined from the PSI and Fd structures using the empirical Moser−Dutton formula[27] (Figures S4−S7 and Supporting Information). This surface is relatively extended and includes the region corresponding to the middle Fd position (red in Figure 2). Although it does not include the regions involved in the alternative Fd positions (blue in Figure 2), it involves other stromal regions, but the corresponding Fd potential docking sites do not contain R39. Therefore the existence of these potential docking sites is not supported by the present BSI experiments.

$K_d$ determinations by BSI and functional ET were in full quantitative agreement. Moreover the present BSI data provide evidence for a single binding site of Fd in PSI. These experiments also show that BSI can be used to probe the interactions between a small protein (Fd, 10.5 kDa) and a large membrane protein (PSI, ~350 kDa) in the presence of detergent and despite the fact that the probing wavelength is strongly absorbed by one of the partners (see Supporting Information).

**Acknowledgment.** B.L. and P.S. thank Véronique Mary for protein purification.

**Supporting Information Available:** BSI principle, assay conditions and prototype design (Figure S1), functional $K_d$ determinations with *Th. elongatus* Fd, redox state of the BSI samples, two titrations curves (Figures S2 and S3), identification of PSI surface for fast Fd reduction (Figures S4−S7), table of BSI titrations. This material is available free of charge via the Internet at http://pubs.acs.org.

## References

(1) Long, H.; Chang, C. H.; King, P. W.; Ghirardi, M. L.; Kim, K. *Biophys. J.* **2008**, *95*, 3753–3766.
(2) Happe, T.; Hemschemeier, A.; Winkler, M.; Kaminski, A. *Trends Plant Sci.* **2002**, *7*, 246–250.
(3) Jordan, P.; Fromme, P.; Witt, H. T.; Klukas, O.; Saenger, W.; Krauss, N. *Nature* **2001**, *411*, 909–917.
(4) Amunts, A.; Drory, O.; Nelson, N. *Nature* **2007**, *447*, 58–63.
(5) Millsaps, J. F.; Bruce, B. D.; Lee, J. W.; Greenbaum, E. *Photochem. Photobiol.* **2001**, *73*, 630–635.
(6) Ciesielski, P. N.; Scott, A. M.; Faulkner, C. J.; Berron, B. J.; Cliffel, D. E.; Jennings, G. K. *ACS Nano* **2008**, *2*, 2465–2472.
(7) Grimme, R. A.; Lubner, C. E.; Golbeck, J. H. *Dalton Trans.* **2009**, 10106–10113.
(8) Sepunaru, L.; Tsimberov, I.; Forolov, L.; Carmeli, C.; Carmeli, I.; Rosenwaks, Y. *Nano Lett.* **2009**, *9*, 2751–2755.
(9) Terasaki, N.; Yamamoto, N.; Hiraga, T.; Yamanoi, Y.; Yonezawa, T.; Nishihara, H.; Ohmori, T.; Sakai, M.; Fujii, M.; Tohri, A.; Iwai, M.; Inoue, Y.; Yoneyama, S.; Minakata, M.; Enami, I. *Angew. Chem.* **2009**, *48*, 1585–1587.
(10) Ihara, M.; Nishihara, H.; Yoon, K. S.; Lenz, O.; Friedrich, B.; Nakamoto, H.; Kojima, K.; Honma, D.; Kamachi, T.; Okura, I. *Photochem. Photobiol.* **2006**, *82*, 676–682.
(11) Ihara, M.; Nakamoto, H.; Kamachi, T.; Okura, I.; Maeda, M. *Photochem. Photobiol.* **2006**, *82*, 1677–1685.
(12) Krassen, H.; Schwarze, A.; Friedrich, B.; Ataka, K.; Lenz, O.; Heberle, J. *ACS Nano* **2009**, *3*, 4055–4061.
(13) Fromme, P.; Schubert, W. D.; Krauss, N. *Biochim. Biophys. Acta* **1994**, *1187*, 99–105.

(14) Lelong, C.; Boekema, E. J.; Kruip, J.; Bottin, H.; Rögner, M.; Sétif, P. *EMBO J.* **1996**, *15*, 2160–2168.
(15) Sétif, P.; Fischer, N.; Lagoutte, B.; Bottin, H.; Rochaix, J. D. *Biochim. Biophys. Acta* **2002**, *1555*, 204–209.
(16) Ruffle, S. V.; Mustafa, A. O.; Kitmitto, A.; Holzenburg, A.; Ford, R. C. *J. Biol. Chem.* **2000**, *275*, 36250–36255.
(17) Jolley, C.; Ben Shem, A.; Nelson, N.; Fromme, P. *J. Biol. Chem.* **2005**, *280*, 33627–33636.
(18) Bornhop, D. J.; Latham, J. C.; Kussrow, A.; Markov, D. A.; Jones, R. D.; Sorensen, H. S. *Science* **2007**, *317*, 1732–1736.
(19) http://www.molsense.com/.
(20) Sétif, P. *Biochim. Biophys. Acta* **2001**, *1507*, 161–179.
(21) Sétif, P.; Bottin, H. *Biochemistry* **1995**, *34*, 9059–9070.
(22) Sétif, P.; Bottin, H. *Biochemistry* **1994**, *33*, 8495–8504.
(23) Cassan, N.; Lagoutte, B.; Sétif, P. *J. Biol. Chem.* **2005**, *280*, 25960–25972.
(24) Barth, P.; Savarin, P.; Gilquin, B.; Lagoutte, B.; Ochsenbein, F. *Biochemistry* **2002**, *41*, 13902–13914.
(25) Barth, P.; Guillouard, I.; Sétif, P.; Lagoutte, B. *J. Biol. Chem.* **2000**, *275*, 7030–7036.
(26) Delano, W. L. *The PyMOL Molecular Graphics System*; DeLano Scientific: 2002.
(27) Moser, C. C.; Dutton, L. *Biochim. Biophys. Acta* **1992**, *1101*, 171–176.

JA102208U